



HAL
open science

Adaptive coherence volume in full-field optical coherence tomography

Naveen Vijayan Mekhileri, Laetitia Andrique, Gaëlle Recher, Pierre Nassoy, Amaury Badon

► To cite this version:

Naveen Vijayan Mekhileri, Laetitia Andrique, Gaëlle Recher, Pierre Nassoy, Amaury Badon. Adaptive coherence volume in full-field optical coherence tomography. *OSA Continuum*, 2021, 4 (11), pp.2805. 10.1364/OSAC.442310 . hal-03427872

HAL Id: hal-03427872

<https://hal.science/hal-03427872>



Submitted on 16 Nov 2022

HAL is a multi-disciplinary open access archive for the deposit and dissemination of scientific research documents, whether they are published or not. The documents may come from teaching and research institutions in France or abroad, or from public or private research centers.

L'archive ouverte pluridisciplinaire **HAL**, est destinée au dépôt et à la diffusion de documents scientifiques de niveau recherche, publiés ou non, émanant des établissements d'enseignement et de recherche français ou étrangers, des laboratoires publics ou privés.



Adaptive coherence volume in full-field optical coherence tomography

NAVEEN VIJAYAN MEKHILERI,^{1,2} LAETITIA ANDRIQUE,³ GAËLLE RECHER,^{1,2}  PIERRE NASSOY,^{1,2} AND AMAURY BADON^{1,2,*} 

¹LP2N, Laboratoire Photonique Numérique et Nanosciences, Univ. Bordeaux, F- 33400 Talence, France

²Institut d'Optique Graduate School & CNRS UMR 5298, F- 33400 Talence, France

³Univ. Bordeaux, TBMCORE VoxCell facility, F- 33076 Bordeaux, France

*amaury.badon@institutoptique.fr

Abstract: Optical sectioning is instrumental for the observation of extended biological samples. It allows the observation of only a slice of the sample while rejecting contributions from out of focus depths. The acquisition of the whole volume then requires an axial displacement of the sample or the focus. To satisfy Nyquist sampling, this axial displacement has to be equal to half the axial resolution. As lateral and axial resolutions are coupled by the numerical aperture of the microscope objective in most imaging techniques, high-resolution imaging of a volume is a time-consuming task, especially caused by the slow axial scanning. Here, we propose to adapt the axial resolution, or axial extent of the coherence volume, by filtering the spectrum of the illumination of an interferometric imaging technique. We applied our approach on full-field optical coherence tomography and show a tuning of this axial extent from 1.5 to 15 μm , allowing to adapt both the acquisition time and the amount of data. We finally demonstrate that the method is especially suited to image large biological samples such as millimetric engineered tissues.

© 2021 Optical Society of America under the terms of the [OSA Open Access Publishing Agreement](#)

1. Introduction

Investigating biomedical engineering questions often requires to observe living specimens over large scales (>1 mm) with a spatial resolution good enough to resolve structures of the order of a micron or even smaller. With its exquisite spatial resolution and relatively low invasiveness, optical microscopy holds a central place in biology and biophysics. The microscope objective (MO) of an optical microscope is considered as the key part as it ultimately dictates the performances of the apparatus such as the magnification of the system, the amount of collected light, the transverse spatial resolution, the field of view (FOV) [1]. For a given MO, these properties are constant and this choice thus critically depends on the specimen or the experiment. For instance, low numerical aperture (NA) objectives usually provide a large FOV and a large depth of field but it comes with a moderate spatial resolution. Alternatively, high NA objectives provide better spatial resolution but at the cost of reduced FOV and depth of field. Thanks to recent progress, some objectives now combine both high NA and large FOV but their price could be prohibiting, especially at building home-made set-ups.

In the last few years, efforts put on the production of more versatile imaging techniques notably with decoupled lateral and axial resolutions or depth of field. Extending the depth of field while keeping a fine transverse spatial resolution is particularly desirable to quickly scan a volumetric sample or to detect fast and sparse events such as calcium activity in brain imaging [2]. Among numerous approaches, several methods proposed to extend axially the illumination beam with point spread function engineering [3], to refocus the detected light with a deformable mirror [4] or to detect signal from multiple depths either spatially [5] or temporally [6].

In this context, we propose here a simple solution to adapt the axial resolution of full-field optical coherence tomography (FF-OCT). By using spectral filters in the illumination path of the apparatus, we show that our technique enables to instantaneously tune the axial extent of the

coherence volume from 1.5 to 15 μm . This allows to image a volumetric specimen quickly with a moderate axial resolution or to image it in details but at the cost of an increased acquisition time and amount of data.

2. Principle and experimental setup

2.1. Axial and lateral resolution in FF-OCT

Optical Coherence Tomography (OCT) is a label-free and three-dimensional imaging technique whose optical contrast relies on the interference between the light back-scattered by a specimen and the light reflected by a mirror in the reference arm (see Fig. 1(c)) [7]. Thanks to its low photo-damage and optical sectioning capabilities, OCT is particularly useful to perform in-depth imaging of biological specimens such as the eye [8,9], the skin [10,11] or more recently engineered tissues [12–14]. In its most-widespread configuration, spectral-domain OCT, a low-NA MO is used to provide a large depth of field for a single pixel acquisition (A-scan). Yet, this extended depth of field also results in a poor lateral resolution, typically around 5 μm . Alternatively, the full-field configuration, denoted FF-OCT, acquires directly a 2D image corresponding to a specific depth (C-scan) [15]. This technique combines the low temporal and spatial coherence of a source to reject the out-of-focus contributions and to achieve crosstalk rejection respectively. This makes it compatible with higher NA objectives and ensures typically a sub-micron lateral resolution which is a clear advantage compared to the spectral-domain version.

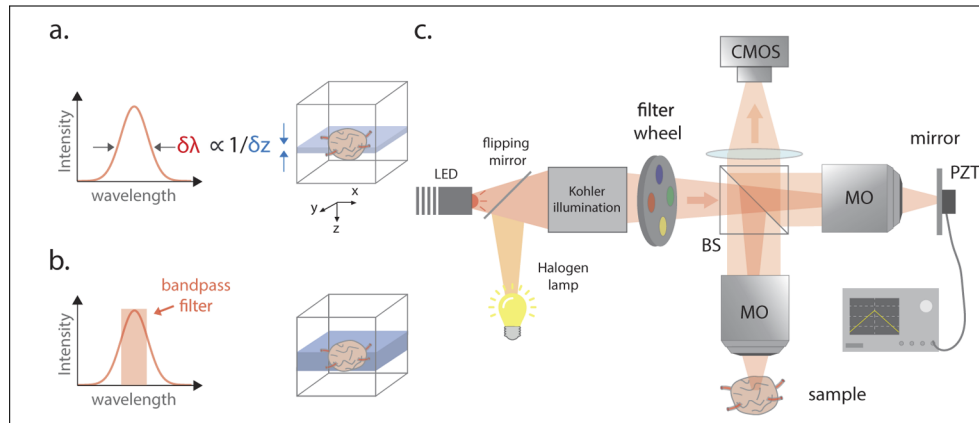


Fig. 1. Principle of tuning the coherence volume in FF-OCT using spectral filtering. (a) In OCT, the axial resolution δz is inversely proportional to the spectral bandwidth $\delta\lambda$ of the illumination source. (b) Reducing the spectral bandwidth of the illumination source extends the axial extent of the coherence volume. (c) Optical setup. A filter wheel containing filter with various spectral bandwidth is inserted in the illumination path of a conventional FF-OCT apparatus. MO, microscope objective; BS, beam splitter; M, mirror; PZT, piezoelectric transducer; LED, light emitting diode.

For the vast majority of imaging techniques, axial and lateral resolutions are intimately coupled and only depend on the light wavelength and the NA of the MO. Because OCT is an interferometric imaging technique this coupling is released here, and the axial resolution is directly given by the coherence length of the source. Indeed, if the optical path length between the two arms is larger than this physical value, the interferences disappear and no signal is obtained. In practice, the coherence length only depends on the central wavelength λ_0 and the bandwidth

$\Delta\lambda$ of the illumination source as following:

$$\delta_z = \frac{2\ln(2)}{\pi} \frac{\lambda_0^2}{\Delta\lambda}. \quad (1)$$

Thus, the axial resolution of a FF-OCT system can be tuned by simply changing the bandwidth of the illumination source and, importantly, without affecting the lateral resolution.

2.2. FF-OCT system with tunable coherence volume

In this work, we developed a FF-OCT system with an axial resolution that can be adjusted according to the sample or acquisition time requirements. In practice, a filter wheel is inserted in the illumination path of a home-made FF-OCT system (see Ref. [13] for more details on the apparatus). Briefly, a broadband and spatially incoherent light source (M660L4, Thorlabs or KL1500, Schott) illuminates a Linnik interferometer in a Kohler configuration made of four lenses and two apertures. Light is separated by a beam splitter (CCM1-BS013, Thorlabs) and propagates through two identical MO (UMPLFLN 10X, Olympus) placed in the two arms. The specimen of interest is placed in the focal plane of one of the MO while a silicon mirror is positioned in the second arm. The latter is supported by a piezoelectric transducer (PZT) which modulates the optical path difference between the two interferometric arms. Light reflected in the two arms is then collected by the same MO, focused by a tube lens (AC508-400-A-ML, Thorlabs) and imaged by a CMOS camera (MV1-D1024E-160-CL-12, PhotonFocus). By combining two light sources and 2 different spectral filters in the filter wheel, our system provides four different spectral configurations :

- (1) Halogen source without any filter ($\Delta\lambda=100$ nm)
- (2) LED without any filter ($\Delta\lambda=17$ nm)
- (3) LED with a 10 nm bandpass filter ($\Delta\lambda=10$ nm)
- (4) LED with a 3 nm bandpass filter ($\Delta\lambda=3$ nm).

3. Results

3.1. Experimental validation of the tunable coherence volume

For each configuration, we estimated the optical performances of the system. Firstly, we investigated the axial resolution by measuring the full width at half maximum (FWHM) of the interferometric signal amplitude with a silicon mirror in both the sample and reference arm (Fig. 2(a-d)). As expected and predicted by Eq. (1), a decrease of the bandwidth of the illumination leads to an increase of the axial resolution. In practice, we measure $\delta_z = 1.5, 4, 10$ and $15 \mu\text{m}$ for the four configurations respectively indicating that the axial resolution can be tuned over an order of magnitude.

To further demonstrate the effect of the spectral filtering on the coherence volume, we replaced the reference mirror in the sample arm by a sample made of $1 \mu\text{m}$ beads sparsely dispersed in an agarose gel. By using the full spectrum of the halogen light, only few beads are visible as the coherence volume corresponds to a thin slice of only $1.5 \mu\text{m}$ (see Fig. 2(a)). When the spectral bandwidth is reduced, an increased number of beads becomes visible on a single frame as the thickness of the slice becomes larger. In addition, OCT acquisitions performed with narrower bandwidths reduce both the data size and the acquisition time. For instance, this reduction factor can be up to ~ 10 with the 3 nm filter compared to the full bandwidth configuration. Importantly, this gain in speed and information does not come with a degradation of the lateral resolution as this parameter depends only on the central wavelength and the NA of the objective.

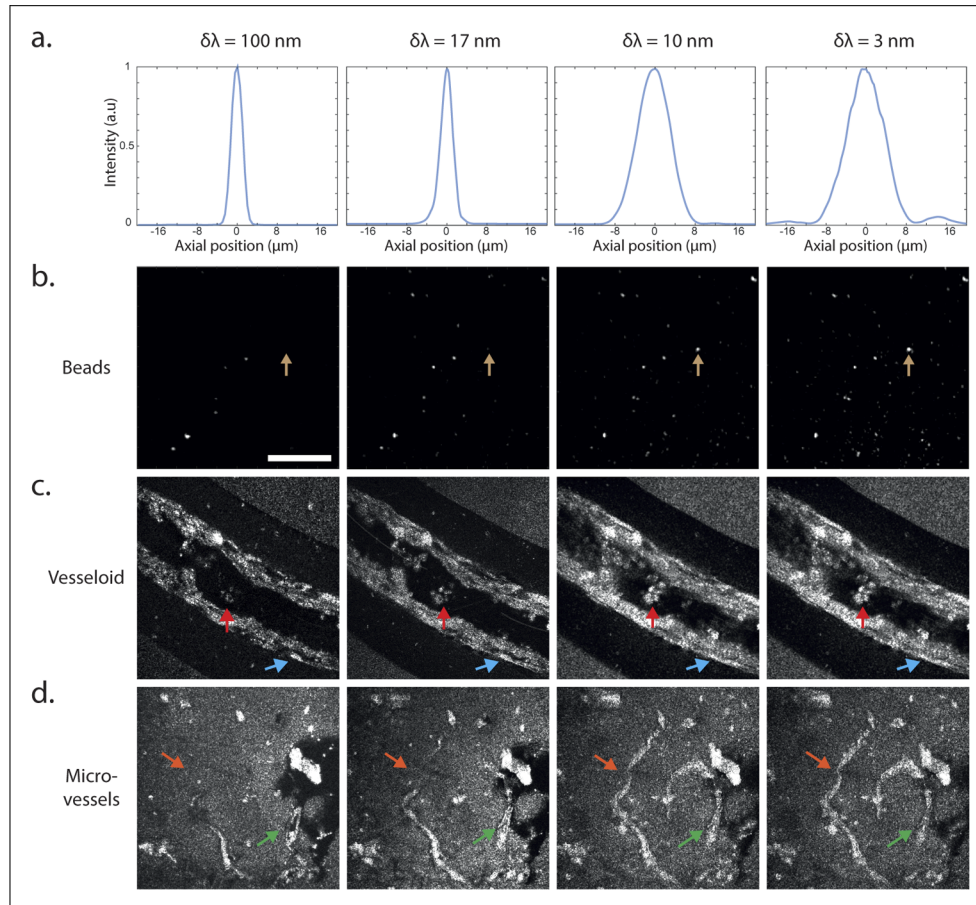


Fig. 2. Effect of the source bandwidth on the axial resolution of a FF-OCT system. (a) Amplitude of the interferometric signal recorded with a silicon mirror in both arms as a function of the optical path difference for $\Delta\lambda=100$, 17, 10 and 3 nm respectively. The resulting axial resolution ranges from 1.5 to 15 μm . (b-d) FF-OCT images obtained with the four same spectral configurations for 1 μm beads embedded in agarose, a vesseloid and endothelial tubes grown in a gelatin matrix. As highlighted by the arrows, the increase of the coherence volume provides more structures of the specimen but the contrast is reduced. Scale bar, 100 μm .

3.2. Demonstration with continuous volumetric specimens : biological engineered tissues

After characterizing the performances of the system in the previous section, we now demonstrate the benefits of our approach by imaging volumetric and complex biological specimens.

We first applied our technique to image a vesseloid (i.e. engineered blood vessel) made of smooth muscle cells and endothelial cells lining on the inner side of an alginate sheath and of about 200 μm in diameter. These samples are of particular interest in the perspective of engineering vascularized tissues [16]. Here, one needs to visualize if this vesseloid obtained by encapsulating a suspension of two types of cells spontaneously forms a lumen, i.e a hollow tubular cell assembly that may be further used to conduct blood diffusing molecules and circulating cells. Figure 2(c) displays the images obtained with the four different spectral configurations. Whereas these images are taken at the same depth ($z=80 \mu\text{m}$), striking differences are visible. With a quasi-isotropic resolution, the broadest spectral bandwidth yields the sharpest, or most contrasted image. The image reveals fine details such as variations of the thickness of the cellular sheet or even the presence of a gap between the two cell population layers. One can note that the dark bands flanking the bright cell signal represent the alginate sheath that is not producing much of signal, whereas the surrounding grey areas correspond to the overall agarose embedding. When the spectral bandwidth of the source is reduced, signal from a larger axial slice is obtained. The vessel wall now appears larger and the contrast is decreased as the image captured an axial projection of structures over a larger slice. For example, the cavity in the tube wall is no longer visible in the 3 nm bandwidth configuration (see blue arrows in Fig. 2(c)). Of course, the extended coherence volume also bears some advantages as more structures are visible on a single image when the bandwidth is reduced. In particular, we notice more supernumerary cells inside the lumen itself as the coherence volume increases (see red arrows in Fig. 2(c)).

Secondly, the same experimental procedure was applied to a sample made of endothelial microvessels. These hollow tubular structures of a few microns-width result from the spontaneous self-organisation of endothelial cells when embedded in a gel that mimics the extra-cellular matrix (GelMA). Such a vascularised gel is of particular interest in the field of tissue engineering as a supporting material to vascularise organoids. This micro-vessels' network, coupled to the vesseloid would provide nutrients to the organoids' core cells. From Fig. 2(d), we observe extending the coherence volume allows to reveal biological structures that are further away the focal plane. Thin vessels from different depths gradually appear as the axial resolution is extended (see orange arrows on Fig. 2(d)). However, this detection of more structures within the sample is accompanied with a reduced contrast. For instance, the lumen of an endothelial tube that is clearly visible with the first spectral configuration disappears when the axial resolution is extended (see green arrows on Fig. 2(d)).

3.3. Stack acquisition

In the previous section, we focused on the effect of the spectral filtering of the illumination source for a single image acquisition. We are now exploring the potential benefits of our technique for the volumetric imaging of a millimeter-scale biological specimen. Here, the specimen of interest is a long vesseloid. The microfluidic process by which the vesseloid is produced allows the extrusion of meter-long tubes [16]. Here, a section of a few centimetres has been wound and embedded in agarose. The inspection of such a structure requires the acquisition of a z-stack that extends over millimeters axially. This results in a time-consuming acquisition and, concomitantly, a large amount of data. In this section, we propose to compare the results obtained with the broader ($\Delta\lambda=100 \text{ nm}$) and narrower ($\Delta\lambda=3 \text{ nm}$) spectral bandwidth configuration with respect to these acquisition parameters.

Acquisition with the narrower spectral bandwidth was first performed. With approximately 15.4 μm axial resolution, a 8 μm axial step is chosen to comply with Nyquist sampling. The

z-stack consists in the acquisition of 200 images spanning 1.6 millimeters. As seen on Fig. 3(a-e), parts of the vesseloid are visible at 5 different depths. Even if the contrast drops as image acquisition goes deeper, the lumen and supernumerary cells inside are still visible. These features are crucial for the characterization of the specimen.

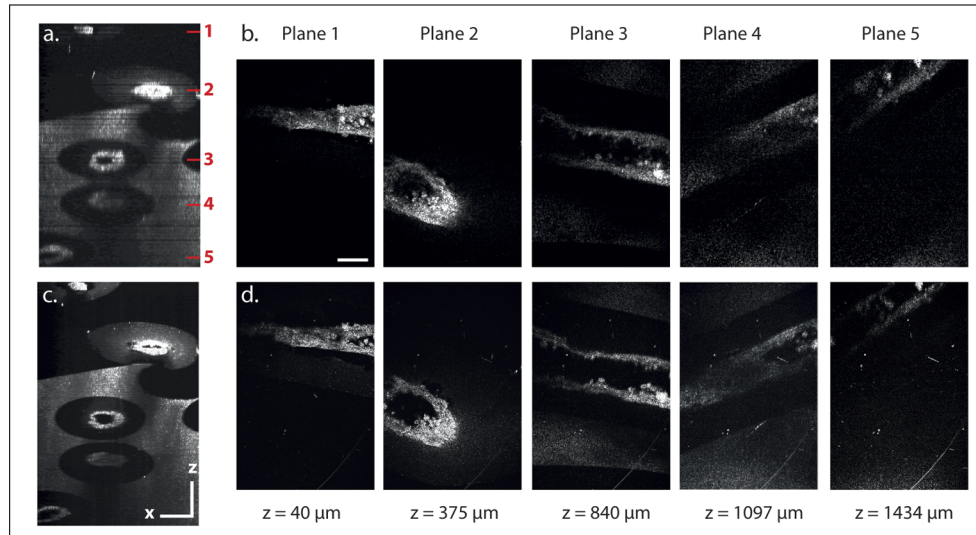


Fig. 3. Performances of the tunable coherence volume method for large volumetric acquisition. (a) Cross section of OCT images acquired with the narrow spectral configuration ($\Delta\lambda = 3$ nm). (b) En face OCT images obtained with the same spectral configuration at five different depths indicated with the red bars in (a). Scale bar, $100 \mu\text{m}$. (c) Cross section of the OCT images acquired with the broad spectral configuration ($\Delta\lambda = 100$ nm). Scale bar, $200 \mu\text{m}$. (d) En face OCT images obtained with the broad spectral configuration at five different depths indicated with the red bars in (a).

Secondly, a z-stack was acquired with the broader spectral bandwidth. A $1 \mu\text{m}$ axial step is chosen to approximately pair with the $1.5 \mu\text{m}$ axial resolution. 1600 images are thus acquired to span the same 1.6 millimeters axial range. As seen on Fig. 3(f-j), the same structures are visible but with a sharper contrast. Yet, compared to the previous configuration, the acquisition time is here 8 times longer (460 minutes compared to 30 minutes) and the amount data is also 8 times larger.

From these results, it appears that the first regime is suitable to quickly identify the regions of interest of an extended sample and to provide qualitative information. The second regime can then be used afterwards for a precise and a qualitative characterization of a subregion of the sample, spotted thanks to the rapid low-res scan, to further examine the cellular disposition within the cell layers.

4. Discussion

In this work we proposed a simple approach to adapt the coherence volume of a FF-OCT system by simply filtering the bandwidth of the illumination source. Our method allows to quickly change the axial resolution from 1.5 to $15 \mu\text{m}$ without generating detrimental effects on the lateral resolution. Yet, the present configuration has also some limitations.

Firstly, our technique only offers a discrete set of values for the axial resolution corresponding to the spectral filters inserted in the illumination path. Continuous tuning of this parameter could

be useful but this requires the use of spectral shapers that will increase the complexity and the cost of the system.

Secondly, filtering the illumination source has obviously a strong impact on the illumination power. If a fraction of the bandwidth is transmitted, a fraction of the source power is also sent to the imaging system. One could think that current LEDs are powerful enough to keep constant the illumination power for the various configurations by adjusting the power emitted by the LED. In practice, we applied a power in the focal plane of each MO equal to 700 μW for the first three configurations. Yet, if the desired bandwidth is too narrow, typically below 2–3 nm, even the brightest LEDs may not be sufficient. In our case, by using the LED at its maximum output power, we measured the power in the focal plane equal to only 600 μW in the last configuration due to the narrow bandwidth. This amount is still comparable with the illumination power measured for the others configurations. If we want to further reduce the bandwidth, the axial resolution of the system will no longer be limited by the coherence length of the source but rather by the depth of field of the MO itself. It means that our approach better suits system with low or moderate NA such as the one used in this study (NA=0.3).

Finally, increasing the axial extent of the coherence volume of a system is particularly appropriate for semi-transparent and sparse specimens. For instance, large axial resolution is interesting for brain calcium imaging as the neurons are distributed over large scales, relatively sparse and the probability to have 2 neurons on top on each other inside the coherence volume is relatively small [4,17]. In the case of label-free continuous samples such as the ones studied in this work, the increase of the spatial information also comes with a decrease of the optical sectioning capabilities and the contrast as contributions from different depths sum up and lower the quality of the image. From this, we believe our technique is of interest for two main applications. The first application is the observation of non-labelled sparse and moving samples, for instance monitoring the circulation of red blood cells inside a vascular network or the motion of a population of small organism such as artemia (*Artemia salina*). Secondly and most importantly, we are convinced that the main potential of our approach is to perform fast pre-scan before a thorough characterization. By increasing the axial extent of the coherence volume, a z-stack containing few frames with a moderate axial resolution is sufficient to target and delineate the regions of interest. In the case of the vesseloid studied in section 3.3, the acquisition with the narrow bandwidth contains sufficient information to detect the five different axial positions of the specimen. Then, a second acquisition with the broader spectral configuration and fine axial step could be performed only at these selected depths. This hybrid imaging method would provide a gain both in acquisition time and in the amount of data without information loss on the sample.

5. Conclusion

In this work, we proposed a simple approach to control and adjust the coherence volume of a FF-OCT system independently of the lateral resolution. With a simple set of spectral filters inserted in the illumination path, the axial resolution can be tuned between 1.5 and 15 μm . In the large axial resolution regime, this allows to extend the coherence volume of the imaging technique which could be useful to track fast three-dimensional events or to quickly probe an extended specimen. In the broader spectral configuration, the low axial resolution mode can then be used to image the fine details with high contrast of an extended specimen.

Funding. Agence Nationale de la Recherche (ANR- 17-CE18-0026-02, ANR- 7-CE30-0007-03, ANR-17-CE13-0012-01, ANR-20-CE19- 0003); Ligue Contre le Cancer (Gironde, Pyrénées); Canceropôle (GSO); Fondation des Treilles.

Disclosures. The authors declare no conflicts of interest.

Data availability. Data underlying the results presented in this paper are not publicly available at this time but may be obtained from the authors upon reasonable request.

References

1. Y. Zhang and H. Gross, "Systematic design of microscope objectives. part i: System review and analysis," *Adv. Opt. Technol.* **8**(5), 313–347 (2019).
2. J. Mertz, "Strategies for volumetric imaging with a fluorescence microscope," *Optica* **6**(10), 1261–1268 (2019).
3. E. R. Dowski and W. T. Cathey, "Extended depth of field through wave-front coding," *Appl. Opt.* **34**(11), 1859–1866 (1995).
4. W. J. Shain, N. A. Vickers, B. B. Goldberg, T. Bifano, and J. Mertz, "Extended depth-of-field microscopy with a high-speed deformable mirror," *Opt. Lett.* **42**(5), 995–998 (2017).
5. A. Badon, S. Bensussen, H. J. Gritton, M. R. Awal, C. V. Gabel, X. Han, and J. Mertz, "Video-rate large-scale imaging with multi-z confocal microscopy," *Optica* **6**(4), 389–395 (2019).
6. D. R. Beaulieu, I. G. Davison, K. Kılıç, T. G. Bifano, and J. Mertz, "Simultaneous multiplane imaging with reverberation two-photon microscopy," *Nat. Methods* **17**(3), 283–286 (2020).
7. D. Huang, E. A. Swanson, C. P. Lin, J. S. Schuman, W. G. Stinson, W. Chang, M. R. Hee, T. Flotte, K. Gregory, C. A. Puliafito, and J. G. Fujimoto, "Optical coherence tomography," *Science* **254**(5035), 1178–1181 (1991).
8. E. A. Swanson, J. A. Izatt, M. R. Hee, D. Huang, C. Lin, J. Schuman, C. Puliafito, and J. G. Fujimoto, "In vivo retinal imaging by optical coherence tomography," *Opt. Lett.* **18**(21), 1864–1866 (1993).
9. V. Mazlin, P. Xiao, E. Dalimier, K. Grieve, K. Irsch, J.-A. Sahel, M. Fink, and A. C. Boccara, "In vivo high resolution human corneal imaging using full-field optical coherence tomography," *Biomed. Opt. Express* **9**(2), 557–568 (2018).
10. E. Aukorius and A. C. Boccara, "Fast subsurface fingerprint imaging with full-field optical coherence tomography system equipped with a silicon camera," *J. Biomed. Opt.* **22**(09), 1 (2017).
11. A. Dubois, O. Levecq, H. Azimani, D. Siret, A. Barut, M. Suppa, V. Del Marmol, J. Malvehy, E. Cinotti, P. Rubegni, and J.-L. Perrot, "Line-field confocal optical coherence tomography for high-resolution noninvasive imaging of skin tumors," *J. Biomed. Opt.* **23**(10), 1 (2018).
12. C.-E. Leroux, F. Bertillot, O. Thouvenin, and A.-C. Boccara, "Intracellular dynamics measurements with full field optical coherence tomography suggest hindering effect of actomyosin contractility on organelle transport," *Biomed. Opt. Express* **7**(11), 4501–4513 (2016).
13. G. Recher, P. Nassoy, and A. Badon, "Remote scanning for ultra-large field of view in wide-field microscopy and full-field oct," *Biomed. Opt. Express* **11**(5), 2578–2590 (2020).
14. S. Wang and I. V. Larina, "In vivo dynamic 3d imaging of oocytes and embryos in the mouse oviduct," *Cell Rep.* **36**(2), 109382 (2021).
15. A. Dubois, L. Vabre, A.-C. Boccara, and E. Beaurepaire, "High-resolution full-field optical coherence tomography with a linnik microscope," *Appl. Opt.* **41**(4), 805–812 (2002).
16. L. Andrique, G. Recher, K. Alessandri, N. Pujol, M. Feyeux, P. Bon, L. Cognet, P. Nassoy, and A. Bikfalvi, "A model of guided cell self-organization for rapid and spontaneous formation of functional vessels," *Sci. Adv.* **5**(6), eaau6562 (2019).
17. R. Lu, W. Sun, Y. Liang, A. Kerlin, J. Bierfeld, J. D. Seelig, D. E. Wilson, B. Scholl, B. Mohar, M. Tanimoto, M. Koyama, D. Fitzpatrick, M. B. Orger, and N. Ji, "Video-rate volumetric functional imaging of the brain at synaptic resolution," *Nat. Neurosci.* **20**(4), 620–628 (2017).